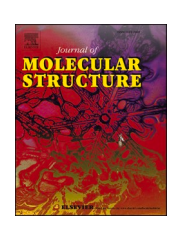
ELSEVIER

Contents lists available at ScienceDirect

Journal of Molecular Structure

journal homepage: www.elsevier.com/locate/molstr





Synthesis, biological evaluation of novel pyridine derivative as antibacterial agent: DFT, molecular docking and ADMET studies

M. Hamsaveni^a, Ruthu Ramachandra Hegde^a, B. Sahana^a, B.S. Chethan^{a,c}, K. Pruthviraj^b, N. Maithra^a, D.C. Vinay Kumar^a, S.V. Niranjana^{a,d}, K. Sunil^b, N.K. Lokanath^{a,*}

- ^a Department of Studies in Physics, University of Mysore, Manasagangotri, Mysuru, Karnataka 570006, India
- ^b Department of Chemistry, Sri Siddhartha Institute of Technology, SSAHE, Tumakuru, Karnataka 572105, India
- ^c Department of Basic Science (Physics), Amruta Institute of Engineering and Management Sciences, Bidadi, Bengaluru, Karnataka 562109, India
- ^d Department of Physics, Karnataka State Open University, Mukthagangothri, Mysuru, Karnataka, 570006, India

ARTICLE INFO

Keywords: Pyridine derivative VEDA analysis DFT Molecular docking Molecular dynamics

ABSTRACT

The diverse pyridine analogues have been reported to display a wide range of biological and pharmacological properties. In our present work, novel 5-methyl-N-(4-methylpyridine -2-yl)-4,5,6,7 tetrahydrothiazolo [5,4-c] pyridine 2-carbaxamide was synthesized and characterized using various spectroscopic techniques such as FTIR and UV-visible. The molecule was optimised using Density functional theory (DFT) based B3LYP calculations with the basis set 6–311 G(d,p). The global reactivity descriptors, HOMO-LUMO orbitals of the molecule were discussed. To evaluate the chemical reactivity and charge distribution, molecular electrostatic potential was carried out. Further, Natural bond orbital analysis (NBO) was determined to study the charge delocalization and hyper conjugative interactions of the molecule. Topological analysis of the compound revealed the information regarding the various intramolecular interactions. In molecular docking study, the inhibitory potential of the molecule was evaluated against the *E.coli* enzymes. The carbonyl group in the compound play a very significant role in antibacterial activity. To study the behaviour of novel compound in living organism and to calculate the physiochemical properties, ADMET analysis was carried out using SwissADME tool. Toxicity was determined by pkCSM online software. Further molecular dynamics studies were performed and the results indicated a good binding affinity of the ligand with the protein during the simulation period of 50 ns.

1. Introduction

The compounds having the heterocyclic frameworks are found to have importance in the pharmaceutical fields such as the material science, agrochemicals etc. [1–5]. This has led to the synthesis of large number of the heterocycle containing compounds. Among the various hetero aromatic architecture, the compounds having the thiazole core exhibits wide range of applications in diverse fields. The thiazole refers to the presence of the sulphur and nitrogen atoms in the aromatic ring. It is found as an essential core scaffold present in many natural and synthetic medicinally important compounds. The thiazole derivatives are found to have good antimicrobial, antitumor, antibacterial, anti-turbercular, anti-HIV, anti-inflammatory and analgesic properties [6–10]. Further, they have been used in agrochemical applications such as herbicides [11] and insecticide [12]. Additionally, the presence of the methyl pyridine group, highlights its significance in the area of

medicinal chemistry. Nowadays, medicinal chemists are investigating new methods for the synthesis of alternative scaffolds that can be used as chemotherapeutic agents in the field of medicinal chemistry. Nitrogen-containing heterocycles are well known for their numerous biological activities and currently play a pivotal role in drug design and drug discovery. Among them, pyridine derivative compounds are privileged pharmacophores that are present in numerous natural products and are tremendously important in biological systems.

In view of the numerous important biological properties of heterocyclic groups we have synthesized novel synthesized 5-methyl-N-(4-methylpyridine-2-yl)-4,5,6,7tetrahydrothiazolo[5,4,c] pyridine 2-carbaxamide compound and it is characterized by the NMR, UV-Visible and FTIR spectroscopic techniques. To explore its chemical and electronic properties we have performed computational studies using density functional theory. The computational studies were performed using hybrid density functional method (B3LYP) with 6-311+(d, p) basis set.

E-mail address: lokanath@physics.uni-mysore.ac.in (N.K. Lokanath).

^{*} Corresponding author.

4-methylpyridin-2-amine

5-methyl-4,5,6,7-tetrahydrothiazolo [5,4-c]pyridine-2-carboxylic acid

5-methyl-N-(4-methylpyridine-2-yl)-4,5,6,7-tetrahydrothiazolo[5,4-c]pyridine-2-carboxamide

Fig. 1. Synthesis scheme of the novel pyridine derivative.

In order to visualize the molecular reactive sites such as electrophilic and nucleophilic regions the molecular electrostatic potential map analysis was performed. Further topology analysis were performed to get deeper insights regarding the intramolecular interactions exhibited by the compound.

2. Materials and methods

2.1. Experimental details

All the reagents and solvents were purchased from Sigma-Aldrich and were used without any further purification. The $^1\mathrm{H}$ and $^{13}\mathrm{C}$ NMR were recorded using Bruker spectrometer of 400 and 100 MHz respectively. The signals are abbreviated as follows: s, singlet; d, doublet; t, triplet; dd, doublet-doublet; m, multiplet. The chemical shifts (δ) were recorded in parts per million using methanol as internal reference. The LC-MS spectra were recorded on an Agilent spectrometer. The FT-IR spectra were recorded in KBr pellets using Perkin Elmer Spectrum IRES from the frequency range of 450–4000 cm $^{-1}$. UV-visible spectra were recorded using Perkin Elmer Lambda 35 spectrophotometer with 20 μg mol $^{-1}$ concentration. The melting points were determined in an open capillary tube.

2.2. Density functional theory

As all the physical and chemical properties of the compounds are related to the electron density distribution, various theoretical studies are extensively used to analyze this electron density distribution. The structure of the synthesized compound is drawn and used as input for the initial approximation to compute the electron wave functions. These wave functions were analyzed using the density functional theory (DFT) using B3LYP correlation functional with 6–311G(d,p) basis set. Using the same level of theory, the geometrical coordinates of the structure was optimized and the absence of the imaginary frequencies indicated that the structure has reached the self consistent ground state configuration.

To get further insight about the electronic properties of the compound, frontier molecular orbitals (HOMO and LUMO), their energy gap was determined using the Koopman's approximation. Further, based on the energy gap various other properties such as the ionization energy, global hardness, global softness, chemical potential and electronegativity etc. were determined. The molecular electrostatic potential (MEP) map analysis reveals the charge distribution and predicts the possible reactive sites exhibited by the compound with the help of the colorcoding ranging from red to dark blue ((nucleophilic regions)) blue>green>yellow>orange>red (electrophilic regions)).

investigate the delocalization or hyper conjugative interactions of the compound natural bond orbital (NBO) analysis were performed. All the calculations were carried out using the Gaussian 16 software [13] and the results were visualized using Gauss view 6.0 program suite.

2.3. QTAIM

The Quantum theory of atoms in molecules (QTAIM) provides a significant amount of information regarding the various intra and intermolecular interactions exhibited by the molecule. The bond critical point (BCP) associated with the presence of the non-zero electron density between the two atoms helps to recognize the interatomic interactions based on the strength and nature of hydrogen bonds [14–17]. Various topological parameters such as the electron density ($\rho(r)$), kinetic energy density (G(r)), potential energy density (V(r)), ellipticity (ϵ) and energy density (H(r)) at the bond critical points of the compound were calculated.

Further, the criteria provided by AIM theory offers a basis to differentiate other interactions from the vander Waal's interactions. The interactions can be classified as follows:

(i) for strong H-bonds ($\nabla^2 \rho BCP$) < 0, HBCP < 0 and covalent in nature (ii) for medium H bonds ($\nabla^2 \rho BCP$) > 0, HBCP< 0 and Partially covalent in nature (iii) for weak bonds ($\nabla^2 \rho BCP$) > 0 and HBCP > 0 and electrostatic in nature [17].

Topology analysis of electron densities at the BCPs were computed. Further more, the RDG (Reduced density gradient) based NCI (non covalent interactions) analysis was carried out. The 2D scatter plot of the s (r) against p(r) provides the information about non covalent interactions. The Hessian matrix of electron density assist to distinguish the interactions as stabilizing ($\lambda_2 < 0$) or destabilizing ($\lambda_2 < 0$).

The formation regarding the electron pair density and the orbitals overlapping owing to the orbital gradient are obtained by the electron localization function (ELF) and localized orbital locator (LOL) analysis. All the above analysis were performed using the Multiwfn software [19] and the visualization of the results were carried out using visual molecular dynamics (VMD) software [18].

2.4. In-silico molecular docking and molecular dynamics studies

Molecular docking is an effective computational tool to explore the interaction of the compound with a specific protein to understand its activity and in the discovery of new drugs for the targeting proteins [18]. The molecular docking study of the synthesized molecule with *E. coli* (PDB:1K2A) were carried out using the MGL tools 1.5.6 with AutoDockVina software [22,19]. The three-dimensional structure of the *E. coli* was downloaded from the protein data bank in PDB format. The

Table 1The vibrational assignment of the theoretical spectra using the VEDA software.

Mode number	Wavenumber (cm ⁻¹)	IR	PED assignments	Mode number	Wavenumber (cm ⁻¹)	IR	PED assignments
1	3801.82	55.07	ν _{NH} (100)	52	1175.17	28.73	ν _{as(NC)} (12)
2	3470.46	7.71	$\nu_{\rm CH}$ (100)	53	1174.65	2.46	τ _{HCNC} (63)
3	3390.45	23.70	ν _{CH} (99)	54	1165.20	65.25	$\nu_{as(NC)}$ (11)
4	3367.87	9.4	ν _{CH} (99)	55	1140.26	14.68	$\nu_{as(NC)}$ (11)
5	3281.82	12.37	ν _{CH} (82)	56	1127.28	3.00	ν _{NC} (19)
6	3275.79	19.49	ν _{CH} (82)	57	1120.35	31.12	τ _{HCCC} (54)
7	3271.80	46.61	ν _{CH} (10)	58	1106.44	1.23	$\nu_{\rm NC}$ (10)
8	3263.24	12.13	ν _{CH} (84)	59	1089.46	15.48	ν _{NC} (29)
9	3252.18	15.48	$\nu_{\rm CH}$ (100)	60	1072.06	6.71	$\nu_{\rm CC}$ (16)
10	3239.79	24.89	ν _{CH} (92)	61	1035.05	3.36	$\nu_{as(CC)}$ (20)
11	3229.49	25.20	ν _{CH} (80)	62	1027.73	10.42	$\nu_{\rm CC}$ (13)
12	3228.99	13.55	ν _{CH} (80)	63	985.55	98.32	τ _{CNCC} (16)
13	3201.98	16.21	ν _{CH} (18)	64	976.80	30.20	δ _{NCO} (31)
14	3138.89	81.55	ν _{CH} (92)	65	943.59	29.83	τ _{CNCC} (33)
15	3124.78	69.09	ν _{CH} (83)	66	911.08	42.27	ν _{SC} (11)
16	3116.23	21.18	ν _{CH} (92)	67	898.07	8.00	τ _{CCCN} (53)
17	1895.26	181.41	ν _{OH} (81)	68	846.69	10.19	ν _{CC} (18)
18	1783.93	3.80	$\nu_{as(NC)}$ (13)	69	833.15	4.97	□ _{NC} (10)
19	1779.26	76.60	$\nu_{as(CC)}$ (21)	70	811.57	1.64	ν _{CC} (25)
20	1743.50	498.32	$\nu_{as(CC)}$ (43)	71	790.45	70.79	τ _{HNCC} (63)
21	1712.56	222.28	ν _{NC} (56)	72	762.91	6.01	OUT _{CCNC} (38)
22	1704.67	186.19	$\nu_{as(NC)}$ (16)	73	746.41	35.20	δ _{CCN} (10)
23	1688.19	4.34	γ _{HCH} (74)	74	672.92	5.57	τ _{CNCC} (10)
24	1678.63	10.23	δ _{HCH} (59)	75	657.04	1.27	ν _{CC} (10)
25	1669.66	14.24	γ _{HCH} (71)	76	622.01	9.82	ν _{SC} (25)
26	1662.04	8.30	γ _{HCH} (74)	77	593.68	2.64	τ _{CCNC} (46)
27	1657.58	1.41	γ _{HCH} (13)	78	573.13	6.52	ν _{CC} (41)
28	1655.75	42.87	δ _{HCH} (59)	79	534.31	21.33	OUT _{CCCC} (51)
29	1631.12	5.71	δ _{HCH} (80)	80	532.61	4.40	δ _{CNC} (17)
30	1629.12	31.67	δ _{HNC} (13)	81	475.11	3.51	δ _{CCN} (25)
31	1621.50	0.05	δ _{HCH} (84)	82	463.63	1.81	δ _{CNC} (48)
32	1581.09	152.19	δ _{HCH} (86)	83	426.06	0.97	δ _{CNC} (48)
33	1570.41	230.57	$\nu_{as(CC)}$ (10)	84	402.62	3.36	δ _{CCN} (13)
34	1549.81	27.92	τ _{HCNC} (12)	85	367.00	2.84	OUT _{CCNC} (47)
35	1523.65	8.68	τ _{HCCC} (51)	86	353.11	10.09	γ _{CNC} (20)
36	1503.35	4.10	τ _{HCCC} (29)	87	347.66	5.07	δ _{CCC} (54)
37	1456.17	277.73	$\nu_{as(CC)}$ (11)	88	305.97	4.13	δ _{CCC} (24)
38	1447.92	7.42	γ _{CNC} (15)	89	289.83	7.63	τ _{CCNC} (27)
39	1424.84	1.79	$\nu_{as(NC)}$ (18)	90	256.91	1.22	τ _{HCNC} (47)
40	1422.04	15.97	γ _{HCC} (15)	91	247.16	2.30	τ _{HCNC} (47)
41	1387.01	29.40	ν _{CC} (30)	92	234.09	0.78	τ _{CNCC} (100)
42	1361.94	155.54	$\nu_{as(NC)}$ (12)	93	212.66	0.33	\square_{SC} (100)
43	1346.82	80.20	$\nu_{as(NC)}$ (12) ν_{NC} (14)	94	161.78	3.99	δ _{CNC} (22)
44	1336.84	10.67	δ _{HCC} (16)	95	158.99	2.12	δ _{CNC} (39)
45	1281.39	5.26	ν _{CC} (10)	96	150.35	0.25	δ _{CNC} (39)
46	1276.38	29.02	ν _{CC} (10) ν _{NC} (27)	97	104.39	3.34	
47	1270.62	29.02		98	72.79	3.34 1.52	τ _{CNCC} (65)
	12/0.62		ν _{NC} (21)	98 99		0.89	τ _{CNCC} (46)
48 49		9.20	δ _{HCH} (12)		58.87		δ _{CCN} (69)
	1236.43	7.95	$\nu_{as(CC)}$ (36)	100	39.60	0.12	τ _{HCCC} (87)
50	1223.63	32.76	δ _{HCH} (15)	101	28.11	1.91	τ _{CNCC} (63)
51	1203.83	7.27	$\nu_{as(CC)}$ (53)	102	12.72	0.02	τ _{NCCN} (80)

Where, ν ; stretching, δ ; in plane bending, γ ; out of plane bending, τ ; twisting/torsion, ν_{as} ; asymmetric stretching.

protein was pre-processed using the AutoDock Tools to remove the heteroatoms and water molecules. Further, the polar hydrogen atoms and Kollman charges were added to the receptor (protein) molecule. The 3D grid was created using AUTOGRID algorithm [20]. The protein-ligand interactions were visualized and the binding sites were analyzed using Biovia Discovery Studio software [23]. Further to study the dynamic stability of the protein ligand complex, molecular dynamics study was performed using the academic version of Desmond modules in Schrodinger 2020-22 suite. The protein 1K2A was prepared using Schrodinger's protein preparation wizard, by removing all the water molecules. Then the inbuilt OPLS3 force field was used to optimize and remove the steric hindrance of the protein. Further, considering the periodic boundary to be orthorhombic system the system was inundated with TIP3P water molecules with a simple point charge. The system is made neutral by the addition of Na+ ions and salt atoms and the resulting protein-ligand system is subjected to 50 ns molecular dynamics simulations with a Marlyna-Tobias Klein barostat and Nose-Hoover

thermostat set to 1 bar and 300 K respectively. The post calculation analysis of the results and visualization is carried out using the Desmond based Schrodinger software suite [21,22].

2.5. Drug likeness prediction and ADME analysis

An ideal drug should not only have a good binding interaction with the target but also need to have good pharmacokinetic properties. Hence to explore the pharmacokinetic properties of the compounds ADMET (absorption, distribution, metabolism, excretion and toxicity) analysis was performed using the Swiss ADME online server [24,25]. The synthesized novel compound was evaluated for its prediction of pharmacokinetic properties, drug similarities. The compound is theoretically evaluated for hydrophilicity, hydrophobicity, solvent accessible surface area, number of rotatable bonds, donor-hydrogen bonds, acceptor-hydrogen bonds, blood brain barrier permeability, Caco-2 cell permeability, human intestinal absorption (HIA), skin permeability to

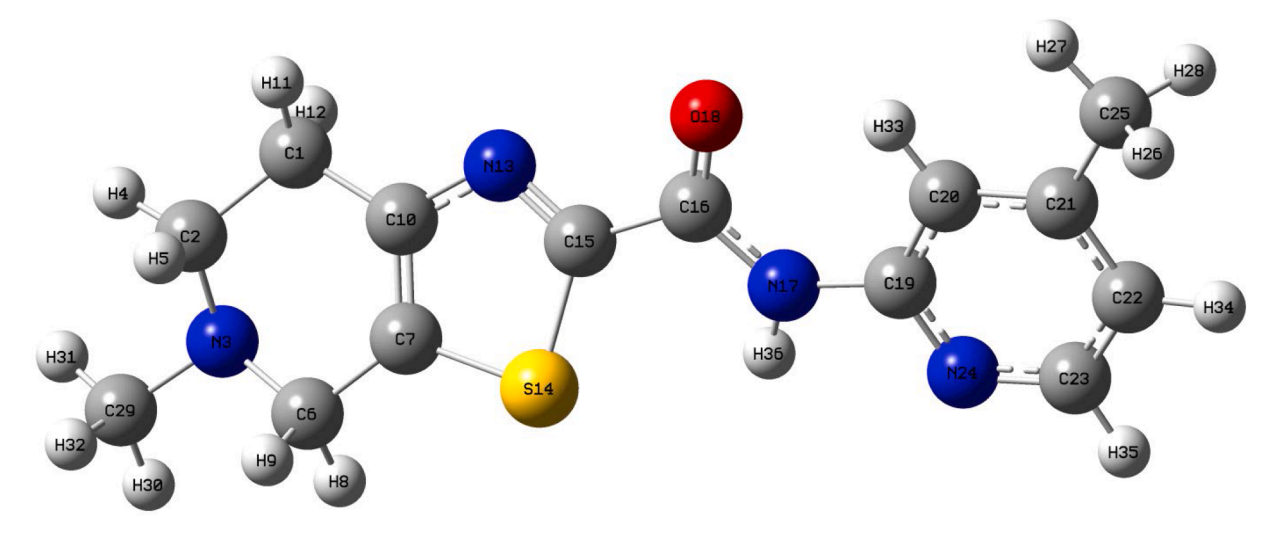


Fig. 2. The ground state structure of the compound optimised at B3LYP level of theory with 6-311G(d,p) basis set.

Table 2The global quantum chemical parameters of the synthesized compound.

Parameters	Values		
E _{LUM0} (eV)	-6.325		
E _{HOMO} (eV)	-1.829		
Energy gap ΔEg (eV)	4.496		
Ionization energy (I) (eV)	6.325		
Electron affinity (A) (eV)	1.829		
Electronegativity (eV)	4.077		
Global hardness (eV)	2.248		
Global softness (eV) ⁻¹	0.445		
Electrophilicity (ω) (eV)	3.697		
chemical potential (eV)	-4.077		

predict important properties based on drug discovery and development.

3. Results and discussion

3.1. Synthesis

To a stirred solution of 5-methyl 4,5,6,7-tetrahydrothiazolo [5,4-c] pyridine-2-carboxylic acid (1.0 eq) in DMF (10 ml) 4-methyl pyridin 2-amine (1.1 eq) was added, and the resultant mixture was stirred at room temperature for 5 min, then N,N-diisopropylethylamine (DIPEA) (2.0 eq) is added. The reaction mixture was cooled to 0 °C then 1-[Bis (dimethylamino)methylene]–1H-1,2,3-triazolo[4,5-b]pyridinium 3-oxide hexafluorophosphate (HATU) (2.0 eq) was added portion wise and the mixture is stirred at room temperature for 3 h.

The reaction mixture was diluted with ice water. The aqueous layer was extracted with DCM. The DCM layer was washed with NaHCO3 solution, collected organic layers were dried over anhydrous sodium sulphate and concentrated under reduced pressure to get crude residue. The crude residue was purified by column chromatography over Silica gel (60–120) using 0 to 100 % Ethyl acetate with nhexane as an eluent to get the desired compound which on evaporation gives 72 % yield of desired compound. The melting point of the compound was determined using capillary method and it is found to be 182–186 °C. The process of the reaction was monitored using thin layer chromatography (TLC). Once the reaction is completed, the resultant product is added to the ice water, filtered and dried to get fine light brown solid (5-methyl-N-(4-methylpyridine-2-yl)–4,5,6,7 tetrahydrothiazolo[5,4-c]pyridine 2-carbaxamide). The Scheme of the synthesis is shown in the Fig. 1.

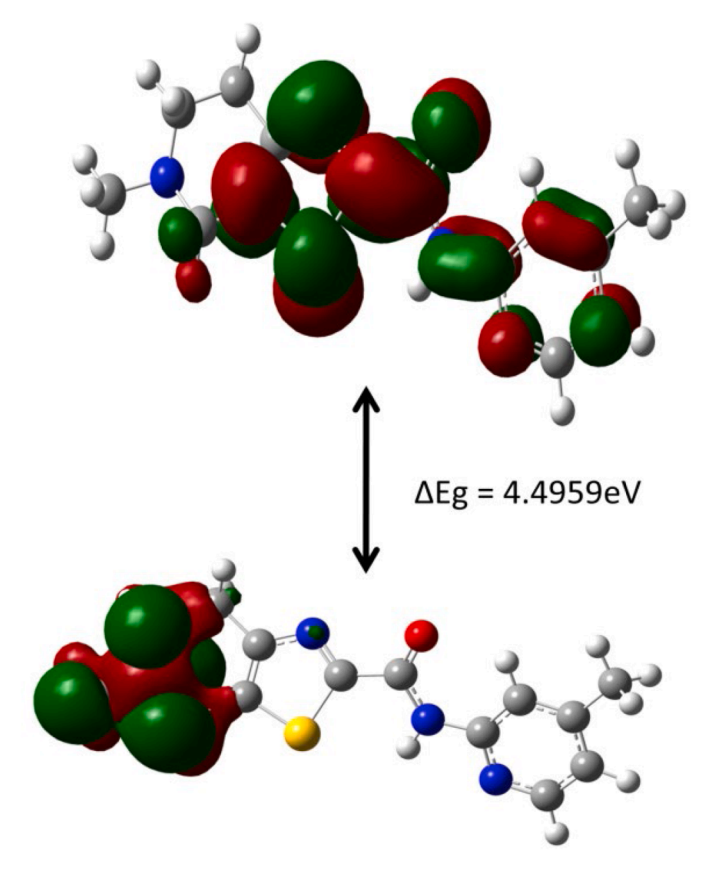


Fig. 3. Frontier molecular orbital distribution on the synthesized compound.

3.2. Spectroscopic characterizations

¹H and ¹³C NMR analysis

 $^1 \rm{HNMR}$ (400 MHz, CDCl₃) $\delta \rm{ppm}$ 1.039-1.106 (6H, s, Ar-CH₃, N-CH₃), 2.48 (4H, s), 3.358 (2H, S), 6.112 (1H,Ar-H), 6.267 (1H,Ar-H), 8.250 (1H,Ar-H). 10.5 (1H,2°-NH)

¹³C NMR (101 MHz, DMSO) δppm 158.771, 156.106, 145.718, 137.131, 134.607, 131.787, 124.464, 123.067, 116.437, 65.433, 60.796, 47.411, 31.490, 22.416.

The presence of 2°-amide NH is located at 10.5 ppm as singlet in ¹HNMR and the highly deshielded carbonyl carbon (C8) adjacent to it

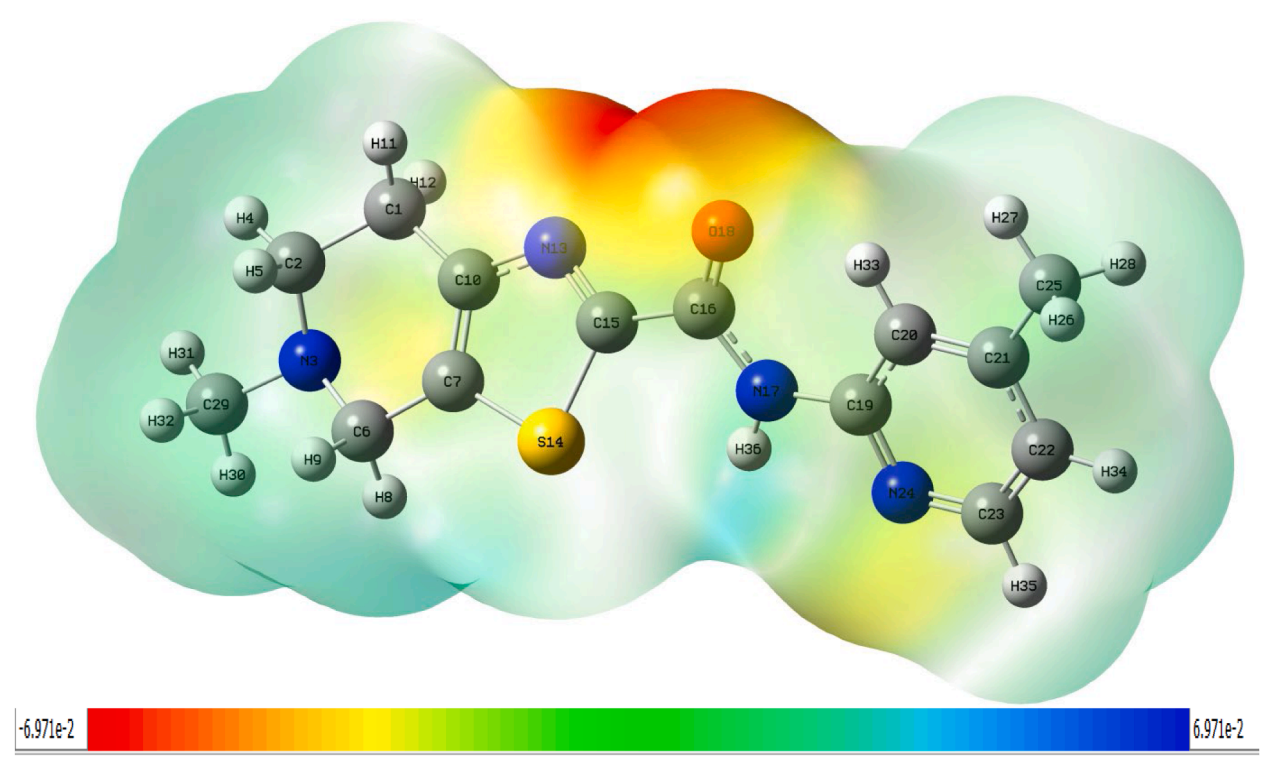


Fig. 4. The molecular electrostatic potential map of the compound revealing the electrophilic and nucleophilic regions.

Table 3Stabilization energy values obtained from the second order perturbation theory analysis of the titled compound.

•		-				
Type	Donor atoms	Occupancy	Type	Acceptor atoms	Occupancy	E ² kcal/ mol
π*	C19- N24	0.45105	π*	C22-C23	0.30231	115.35
π*	N13- C15	0.36309	π*	C16-O18	0.29274	109.72
π*	C19- N24	0.45105	π*	C20-C21	0.31193	100.44
π*	N13- C15	0.36309	π*	C7-C10	0.29665	77.71
LP (1)	N17	1.6569	π*	C16-O18	0.29274	56.53
LP (1)	N17	1.6569	π*	C19-N24	0.45105	39.82
П	C20-C21	1.6531	π*	C19-N24	0.45105	31.85
П	C19- N24	1.71916	π*	C22-C23	0.30231	27.28
LP (2)	S14	1.61307	π*	N13-C15	0.36309	26.21
LP (2)	018	1.85274	σ*	C16-N17	0.07724	24.83
П	C22-C23	1.66902	π*	C20-C21	0.31193	24.38
LP (2)	O18	1.85274	σ*	C15-C16	0.0823	20.89

appears at 158.77 ppm, 2 methyl groups are appeared as merged in proton NMR accounting for 6protons, shown as different peaks in the ¹³CNMR spectrum at 22.416 (C14) ppm and 47.411 ppm (C1), 4 aliphatic protons of fused tetrahydro pyridine appears at 2.48 ppm, whereas protons attached to C2 appears at slightly upfielded giving sufficient data for the formation of desired molecule.

The 1H and 13C NMR of the synthesized compound is shown in the Figs. S1 and S2 respectively.

3.3. FT-IR analysis

FTIR is one of the spectroscopic methods with extensive application of the identification of the presence of various types of bonds in molecules. The theoretical FTIR calculations were carried out using DFT B3LYP method 6–311G (d,p) basis set. The FTIR spectra of the synthesized compound were obtained in the range 400–4000 cm $^{-1}$. The theoretical and experimental FTIR spectra of the titled compound are shown in the Fig. S3. Further, potential energy distribution (PED) analysis was performed using VEDA4 program to understand the contribution of various vibrational modes to the total vibrational energy. The detailed description of the each of the normal mode [(3N-6), where N is the number of atoms in the molecule] vibration carried out for the compound in terms of the potential energy contribution is given in the Table 1.

The absorption band observed in the region 3584.96 cm⁻¹ indicates the N-H stretching modes which is in the range of 3300–3600 cm⁻¹. The PED for this mode suggested that it is a pure stretching mode. The C-H frequencies were found to be in the range between 3100 and 3000 cm⁻¹ and for our compound the C-H peak corresponds to the wavenumber of 3098.12 cm⁻¹. The PED analysis for this mode of vibration indicated that the C-H is exhibiting symmetric stretching vibration. The C=O stretching vibration of the compound was observed at 1761.68 cm⁻¹. The PED analysis suggested that the CH₂ exhibited in plane bending at 1678.63 (59 %), 1655.75 (59 %), 1631.12 (80 %), 1621.50 (84 %) and 1581.09 (86 %). Further the out of plane vibrations of the CH₂ moiety and its corresponding PED values observed in the molecule at 1688.19 (74 %), 1669.66 (71 %), 1662.04 (74 %) and 1657.58 (13 %). Further, the CCCH exhibited torsion at 1523.65 and 1503.35 cm⁻¹ with the contribution of 51 and 29 % respectively. The IR and PED values corresponding to the modes of vibrations are provided in the Table 1 [30, 31].

3.4. UV-visible analysis

UV-visible analysis was carried out to understand the nature of

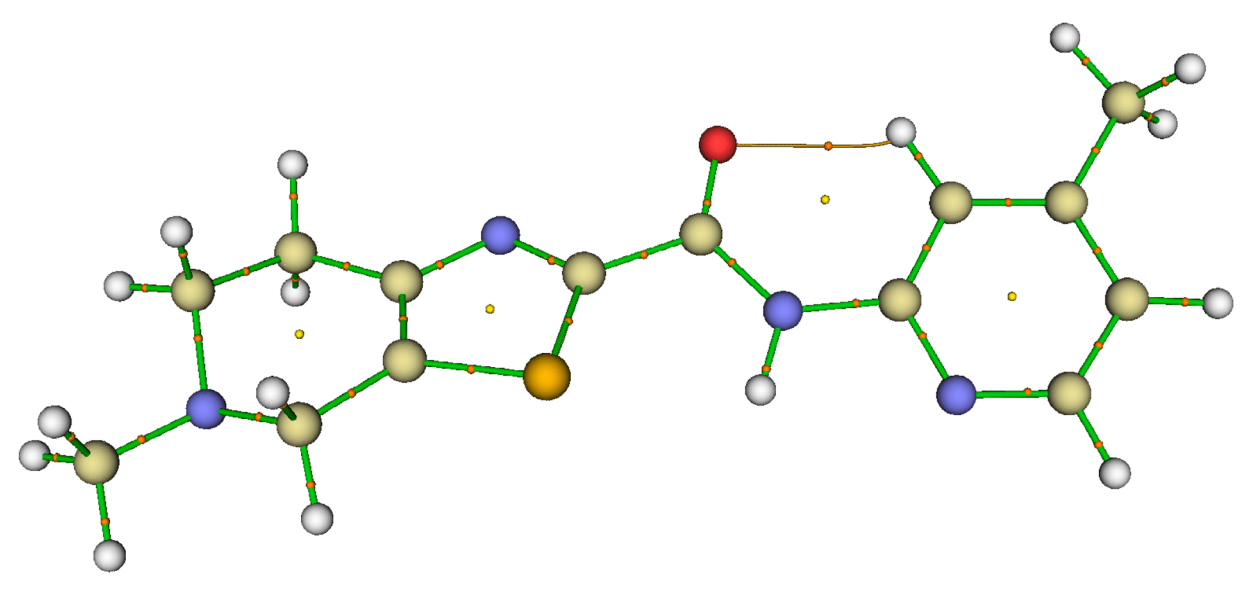


Fig. 5. . The molecular graph of the compound revealing the intramolecular interaction associated with the bond critical points.

Table 4QTAIM based topological properties of the synthesized compound.

Interactions	$ ho_{\mathrm{BCP}}$	G_{BCP}	V_{BCP}	ε	$^{igtitarrow 2} ho_{ ext{BCP}}$	H_{BCP}	V /G
O18 – H33	0.01728	0.01354	-0.01149	0.10666	0.06240	0.00205	0.84859

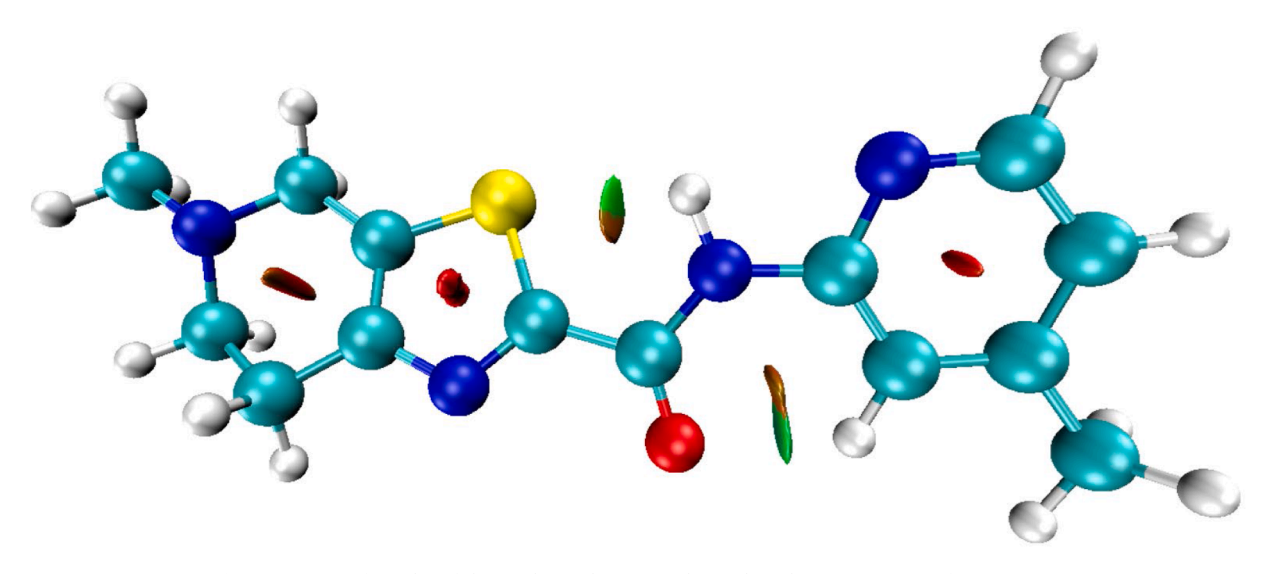


Fig. 6. 3D Isosurface plot of the synthesized compound revealing the various types of interactions.

electronic transitions within a molecule. The UV-visible absorption spectra were recorded at temperature with 20 $\mu gmol^{-1}$ concentration solutions in acetonitrile for the wavelength range of 200–400 nm. The electronic absorption spectra were also calculated using TD-DFT calculations with CAM-B3LYP functional at the 6–311 G (d,p) level basis set. The compound showed a absorption peak in the region of 309.74 nm. The peaks in the region of 330–341 nm are assigned to the single electron π^* - π^* transition in the aromatic ring and the conjugation of the molecule [23]. The UV-visible plot of the compound is shown in the Fig. S4.

3.5. Quantum computational studies

3.5.1. Density functional theory

To get the deeper insights into the electronic properties of the synthesized compound, the geometrical coordinates of the synthesized compound is optimized using the DFT. The absence of the imaginary frequencies indicated that the compound is in the true ground state configuration. The optimized structure of the synthesized compound is given in the Fig. 2.

3.6. HOMO-LUMO and reactivity analysis

The HOMO (highest occupied molecular orbital) –LUMO (lowest unoccupied molecular orbital) energy gap is an good indicator of the

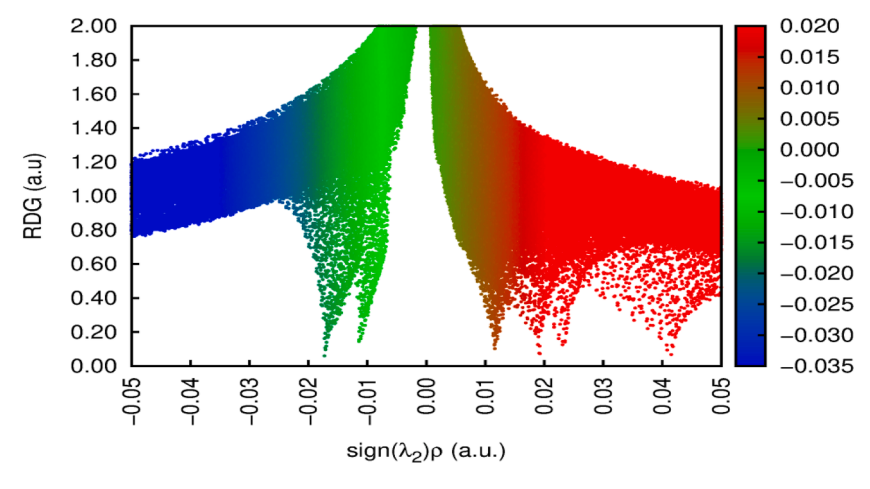


Fig. 7. 2D scatter plot of the titled compound.

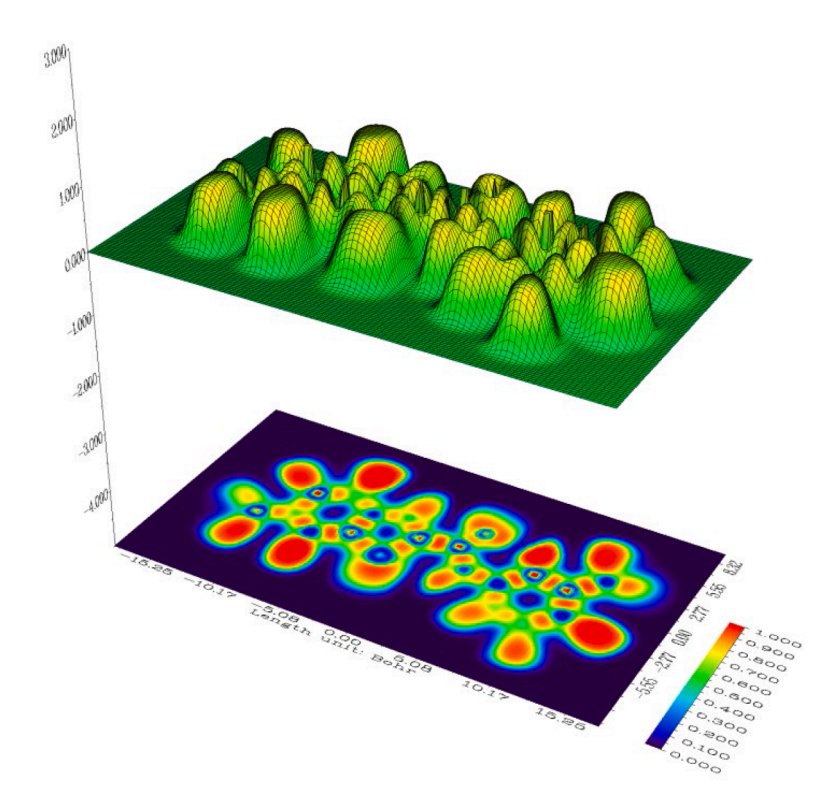


Fig. 8. Colour filled electron localized function with projection map of the synthesized compound.

chemical reactivity of the compound. Smaller the ΔEg more will be the reactivity of the compound [26,27]. The reactivity tendency of one molecule with another molecule is discussed based on the hard-soft-acid-base rule. As usually the biological targets such as the cell, proteins are soft and they cna easily interact with the soft molecules [29]. Thus the biological activity of the compound increases with increase in the softness and decreasing hardness values. The HOMO-LUMO energy gap (ΔEg) of the compound is found to be 4.496 indicates the charge transfer interaction in the molecule and reflects the biological activity of the compound [30]. Higher the value of the electrophilicity index and low value of the chemical potential favours the electrophilic behaviour [32,33]. From Table 2 it is evident that for the compound under investigation, the electrophilicity value is found to be 3.697 eV which is greater than the chemical potential value (-4.07 eV) thus confirming the electophilic behaviour of the compound [29].

The highest occupied (EHOMO) and lowest unoccupied (ELUMO)

energies of the molecular orbitals reveal many important parameters such as energy gap (Δ Eg), ionisation energy (I), electron negativity (χ), electron affinity (A), chemical potential (μ), global hardness (η), global softness (s) and electrophlicity (ω) of the synthesized compound, and these parameters are listed in the Table 2. E_{HOMO} indicates the electron donating ability of the molecule. Whereas, E_{LUMO} denotes the ability of the molecule to receive electrons. Energy gap is a good indicator of stability and reactivity of the compound. Larger the energy gap, greater will be the molecular stability, aromaticity and lesser will be its chemical reactivity.

The distribution of the frontier molecular orbitals are shown in the Fig. 3. The highest occupied molecular orbitals are found to be distributed over the methyl pyridine group, whereas the lowest unoccupied molecular orbitals are distributed over the thiazolopyridine carboxamide group. The energy difference between the HOMO and LUMO orbital is found to be 4.496 eV, it indicates that the molecule is stable,

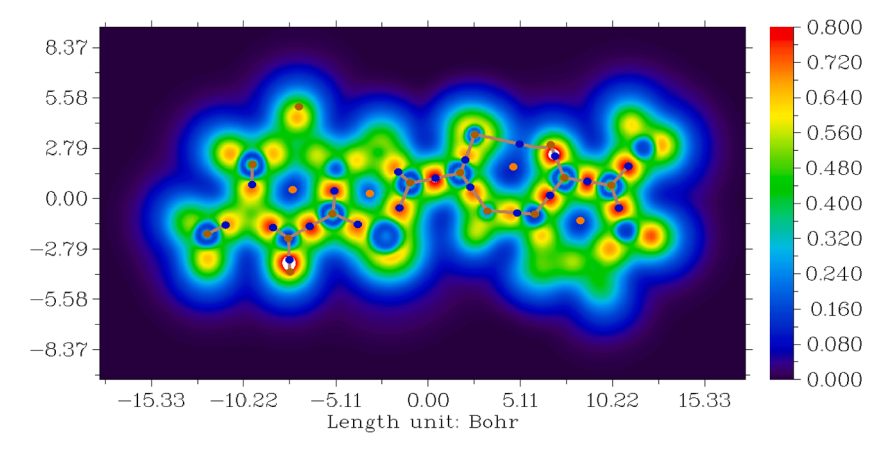


Fig. 9. Localized orbital locator of the titled compound.



Fig. 10. 3D interactions of the synthesized compound with E.coli protein.

hard and is chemically less reactive. The global quantum chemical frontier molecular orbital energy descriptors enable us to know the chemical properties of the compound [34,35].

3.7. Molecular electrostatic potential

The electrostatic surface potential map are very useful to visualize the charge distribution on the molecule in terms of colour grading. Further, it gives the information about the physiochemical features of the molecules and reveals the electro positive and electronegative regions associated with the molecule. These regions helps us to identify the potential regions for binding. The different values of electrostatic potential are represented by distinct colours. The electrophilic and nucleophilic areas are denoted by red and blue colours respectively. The MEP map of the synthesized compound along with the values are shown in Fig. 4. The red region on the oxygen atom of the carbonyl group indicates the electrophilic nature, making it susceptible to nucleophilic attack.

3.8. Natural bond orbital analysis

To understand and study the chemical characteristics of the bonding such as inter and intra molecular interactions, hyperconjugation and stabilization energy of the molecule the NBO analysis was performed. The stabilization energies ($E^{(2)}$) between the donor, lone pairs, acceptor and non-Lewis NBOs, were estimated using the second order perturbation approach and larger the $E^{(2)}$ value, the greater will be the conjugation exhibited by the system.

The strong intramolecular hyper conjugation interactions of the lone pair, σ and π electron systems lead to the stabilization of bonding or antibonding orbitals. The NBO analysis revealed that the hyper conjugative interactions were formed due to the overlap of the orbitals between $\pi^*(C 19 - N 24) \rightarrow \pi^*(C 22 - C 23)$, $\pi^*(N 13 - C 15) \rightarrow \pi^*(C 16 - O 18)$, $\pi^*(C 19 - N 14) \rightarrow \pi^*(C 20 - C 21)$ and $\pi^*(N 13 - C 15) \rightarrow \pi^*(C 7 - C 10)$ anti bonding orbitals with stabilization energies 115.35,109.72, 100.44 and 77.71 kcal mol $^{-1}$ respectively. In addition, the lone pair orbitals LP(1)(N 17) $\rightarrow \pi^*(C 16 - O 18)$ (56.53 kcal mol $^{-1}$) and LP (1) (N 17) $\rightarrow \pi^*(C 19 - N 24)$ (39.82 kcal mol $^{-1}$) also contributes towards the stabilization of the molecule (Table 3).

3.9. Topology analysis

3.9.1. QTAIM analysis

Bader's quantum theory of atoms in molecules is widely used to understand the intra and inter molecular interactions present in the molecule. Topological analysis was performed to study the nature of bonds in a molecular system based on the electron density at specific points called BCPs. The electron density in BCPs indicates the strength of the bond between two atoms. The molecular graph obtained from the optimized structure of the synthesized compound as shown in Fig. 5.

In our compound the BCPs are generated between O18 and H33 atoms. The strength and type of bond present in a compound is characterized by the topological parameters such as electron density (ρ) , Lagrangian kinetic energy (G), potential energy (V), Laplacian of electron density $(\nabla^2\rho)$, ellipticity of electron density (ϵ) and total electron energy density (H) at the critical points. The QTAIM Properties of the titled compound at BCPs are given in the Table 4.

3.10. NCI-RDG analysis

The NCI-RDG analysis enables the graphical visualization of the regions where the non covalent interactions occur. The colour scheme of blue-red-green helps in the identification of nature and type of interactions exhibited by the molecule. To characterize the type of interactions present in the molecule, NCI isosurface analysis was performed which revealed many different interactions which were not shown in molecular graph analysis. The NCI isosurface graph of the

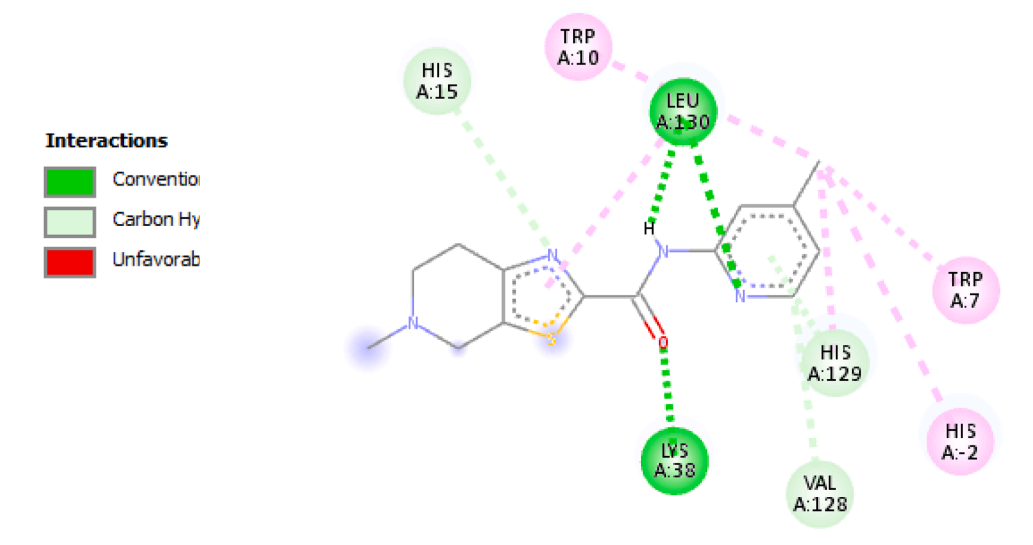


Fig. 11. 2D binding interactions of the titled compound with E.coli enzyme.

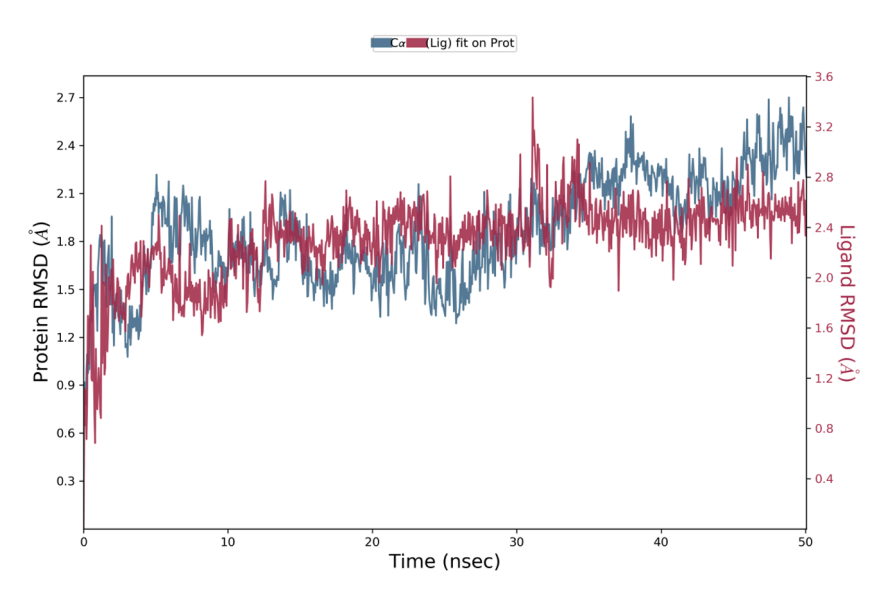


Fig. 12. RMSD plot of the protein-ligand complex indicating the good stability of the complex throughout the simulation period of 50 ns.

novel compound is shown in Fig. 6. The red and green colour indicates that the repulsive and attractive interactions between the atoms respectively. The attractive interactions evidenced by the green patches present between the (S14-H35) and (O18-H33) atoms. This indicates the presence of van der Waals interactions and also attractive nature exist between the molecules. The red region present in the middle of ring indicates steric repulsion between the atoms.

The 2D scatter plot confirms the presence of various interactions. In 2D plot the blue, green, and red colour spikes are shown. The red spike indicate the steric repulsion observed in the middle of the cage, which is due to the steric repulsive force between the atoms. The red green mixed spikes observed in the scatter plot confirms the presence of the interactions between the hydrogen atoms with neighbouring atoms. The RDG scatter map of the compounds shown in the Fig. 7.

The strong steric effect inferred from the RDG isosurface, are inferred by the spikes observed in the regions 0.01 to 0.04 a.u. Whereas, the green spikes observed in the regions -0.01 to -0.02 a. u. indicates the van der Waals dispersion forces exhibited by the molecule.

3.11. Electron localization function and localized orbital locator analysis

Electron localization function (ELF) analysis is used to estimate the electron localization between atoms [24,29]. It provides an idea about the chemical structure, molecular bonding, reactivity and the possibility of finding an electron with the same spin in the neighbourhood of a reference electron. The colour scheme of red and blue indicates the localization and delocalization of electrons respectively. The ELF map of the synthesized compound is given in the Fig. 8. The red regions are associated with the hydrogen atoms indicates that the electron are highly localized. Whereas, the blue regions indicates the delocalization of electrons. The high LOL values of the covalent type of electron depletion region around the nitrogen atom are given in red color. The localized orbital locator of the synthesized compound is given in the Fig. 9.

3.12. Molecular docking and molecular dynamics studies

The binding pattern of the titled compound with the protein molecule were simulated using AutoDock program to validate their structureactivity relationships. The 3D crystal structure of the protein (PDB ID:

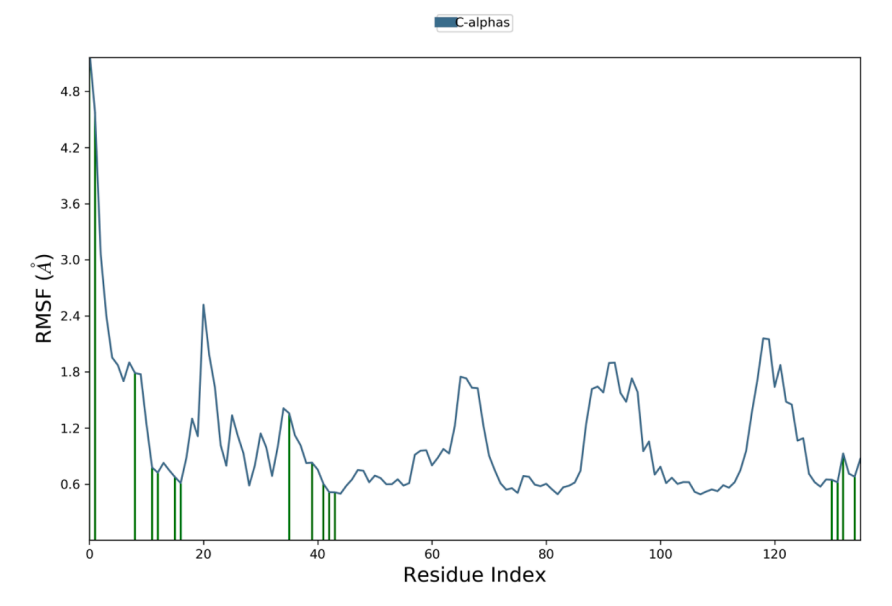


Fig. 13. The RMSF plot with the green vertical lines indicating the fluctuations of the amino acids interacting with the ligand during the simulation period.

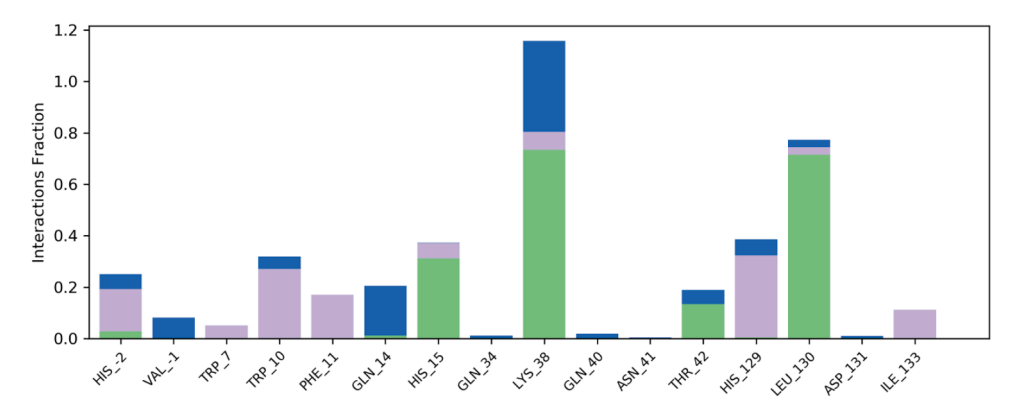


Fig. 14. The Histogram plot revealing the type of interactions exhibited by the amino acids with the protein. (Green: hydrogen bond interactions, grey: hydrophobic type of interactions and blue: water bridges).

1K2A) was obtained from the protein data bank [25–26,32]. Protein ligand preparations has been carried out from the Autodock. The ligand protein docked complexes were analyzed and the best pose selection is associated with the docking pose with the lowest binding energy value and its bonding interaction pattern with the active regions of enzymes. The protein ligand interaction is mainly due to the $\pi-$ alkyl (residues TRPA:7, HISA:-2) and $\pi-$ T shaped (residues TRPA:10) interactions. The docking score of the complex is found to be -8.1 k cal/mol. The 3D docking pose of the ligand with the protein and 2D interaction of the ligand and protein is given in the Figs. 10 and 11 respectively. It reveals the interaction of the compound with the amino acid residues of the protein.

To further investigate the binding mode stability of the protein-ligand complex, molecular dynamics simulations was performed. The stability of the protein-ligand complex system is studied by analyzing various parameters such as RMSD, RMSF and protein-ligand interactions during the simulation period of 50 ns. The root mean square deviation of both the protein and the ligand as shown in the Fig. 12 indicates a good stability of the ligand within the binding pocket of the protein for the simulation period of 50 ns. Both the protein and ligand fluctuations are found to be well within 2.7 Å indicating the minimum fluctuations in the binding region.

The root mean square fluctuations of the protein-ligand complex which provides additional information regarding the interaction of amino acids in contact with the ligand is shown in the Fig. 13. The green colored lines indicates the amino acids in contact with the ligand and the amino acids involved in the interactions are found to be HIS2 (4.3 Å), VAL1 (1.8 Å), TRP7 (0.7 Å), TRP10 (0.67 Å), PHE11 (0.61 Å), GLN14 (0.6 Å), LYS38 (1.3 Å), GLN40 (0.7 Å), ASN41 (0.6 Å), THR42 (0.58 Å), HIS129 (0.56 Å), LEU130 (0.61 Å), ASP131 (0.59 Å) and ILE133 (0.6 Å). Except for the HIS2 amino acid all other amino acids are found to be having less fluctuations with that of the ligand indicating that the forces around the ligand in the binding cavity is favourable for it persist during the simulation period. The type of the interactions exhibited by these amino acids with the ligand is also explored using the histogram plot. The amino acids HIS2, GLN14, HIS15, THR42, LEU130 exhibited hydrogen bond interactions (green color). Whereas most of the amino acids (HIS2, TRP7, TRP10, PHE11, HIS15, LYS38, HIS129, ILE133) echibited hydrophobic interactions as indicated by the grey color in the histogram plot. The amino acids interacting with the ligand through water bridges is shown by the blue color in the Fig. 14.

Other properties of the ligand explored during the simulation period such as the RMSD of the ligand, rGyr (radius of gyration), MolSA (molecular surface area), SASA (solvent accessible surface area) and PSA (polar surface area) (Fig. 15). The RMSD of the ligand showed stable value averaged at 1.5 Å, no significant change in the rGyr value of the protein ligand complex was observed with the fluctuations averaged at 4.12 Å. No intramolecular hydrogen bond formation was observed

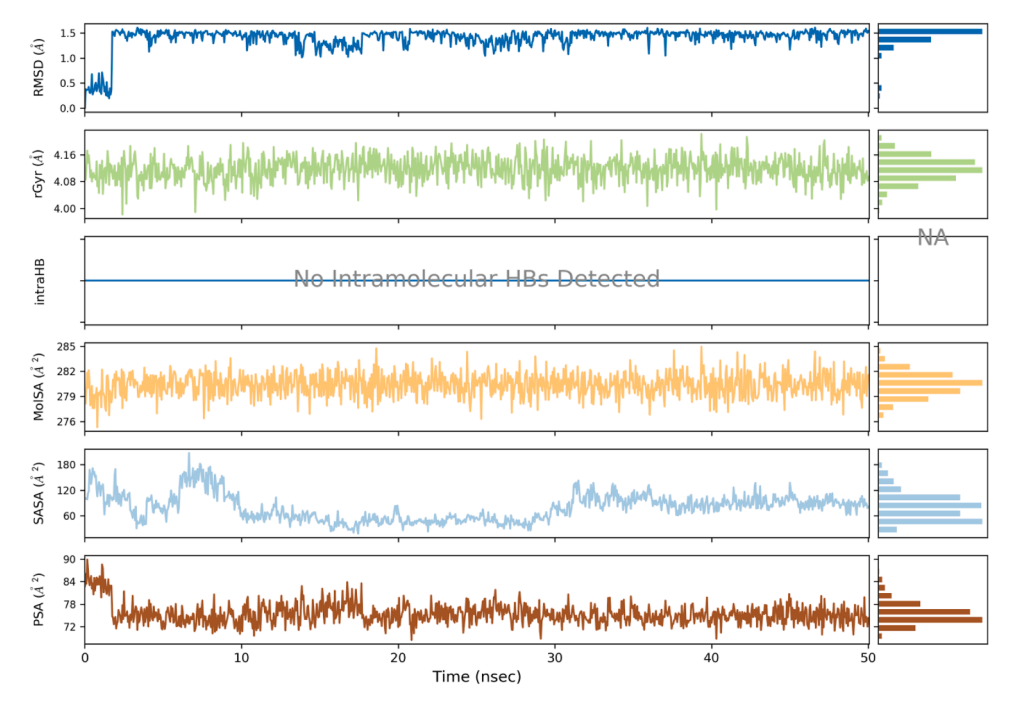


Fig. 15. Various properties of the ligand explored during the simulation period of 50 ns.

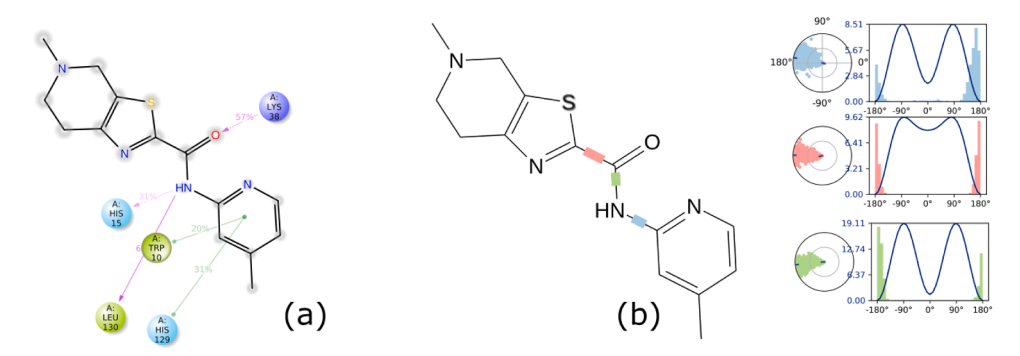


Fig. 16. (a) Fingerprint plot of the compound and (b) 2D dial plot along with the torsional plot.

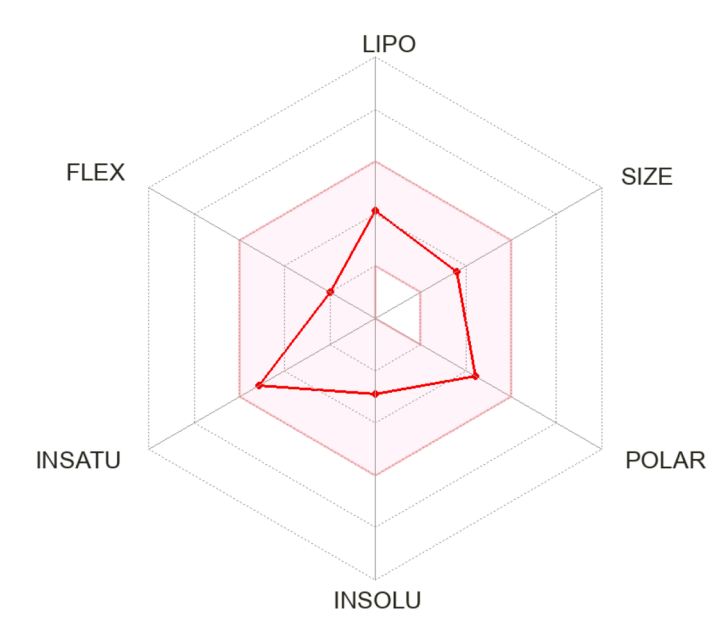


Fig. 17. Bioavailability radar of the synthesized compound.

Table 5Physiochemical properties of the novel compound.

Molecular weight (MW)	-288.37 3		
	3		
No. of rotatable bonds			
Hydrogen bond acceptors	4		
Hydrogen bond donors	1		
ilogP	1.90		
LogS	-2.9		
TPSA	86.36		
Molar refractivity	83.33		

during the simulation period. In-depth solvent accessible surface analysis was performed to analyze the changes in hydrophobic and hydrophilic residues. The MolSA, SASA and PSA values are found to be averaged at 281, 100 and 74 $\mbox{\normalfont\AA}^2$ respectively.

The interaction between the ligand and the protein is highly direction specific in nature hence to understand this relation the dial plot of the ligand is analyzed. The 2D dial plot with different color code corresponding to the color in the particular bond in the ligand gives the angles for each bond at a given time during the simulations. The 2D fingerprint plot, dial plot and the histogram are shown in the Fig. 16.

Table 6
Pharmacokinetics properties of our compound evaluated using SwissADME tool.

Parameters	Pharmacokinetics		
GI absorption	High		
BBB permeation	No		
P-gp substrate	Yes		
CYP1A2	Yes		
CYP2C19	No		
CYP2C9	No		
CYP2D6	No		
CYP3A4	Yes		
Log K _p (skin permeation)	-6.86		

3.13. ADMET analysis

The ADMET parameters disclose the behaviour of chemical compounds in a living organisms. The physiological parameters of the synthesized compound reveals that it obeys Lipinski rule of five (no parameters are violated) which shows good bioavailability (bioavailabity score = 0.55). Bioavailabilty radar of our compound is shown in the Fig. 17. In the graph pink area within the hexagon represents the optimal range of each property. The parameters such as XLOGP3 = 1.69 (-0.7 to +5.0), molecular weight = 288.37 g/mol (150–500 g/mol), polar = 86.36 (20 and 130 A^2), solubility (LogS) = -4.37 (logs not higher than 6), flexibility (FLEX) = 3 (not more than 9 rotatable bonds), saturation (INSATU) = 0.11 (not less than 0.25) of our compound has within the acceptable range. The physiochemical properties of the titled compound is given in the Table 5. The ADMET results of the titled compound are interpreted as it shows high gastrointestinal absorption and also high skin permeability. P-glycoprotein substrate and inhibitory activity was also determined and it is shown in Table 6 (pharmacokinetic properties). The BOILED-Egg model of our compound is shown in the Fig. 18. In the figure we observed that our compound lies in the white region, which suggests that the compound having the highest probability of being absorbed by the gastrointestinal tract [27,28].

4. Conclusion

In the present research work we have synthesized 5-methyl-N-(4-methylpyridine -2-yl)-4,5,6,7 tetrahydrothiazolo [5,4-c]pyridine 2-carbaxamide compound with good yields and characterized by various analytical and spectroscopic techniques. The structure of the compound was optimized using DFT at B3LYP level of theory. The energy gap of the

compound is found to be 4.496 eV indicating that the compound is stable. The MEP analysis revealed that the electrophilic region exhibited by the compound (around the oxygen atom) which provides the information regarding the directionality of the nucleophilic attack by the other chemical species. This information is vital in understanding the approach of the molecule while interacting with the proteins.

The NBO analysis revealed that the transfer of the lone pair of charges from the N17 to the antibonding orbitals of the C16-O18 is found to be associated with stabilizing energy of 56.53 kcal/mol, which indicates the intramolecular charge transfer exhibited by the compound. The topology analysis revealed that all the intramolecular interactions exhibited by the compound are associated with the van der Waals force contributing majorly towards the stability. Further, the molecular docking with the E.coli showed substantial binding affinity of the ligand with docking score of -8.1 kcal/mol indicating the compound to possess very good antibacterial activity. The ADME predictions revealed that the titled compound shows good drug likeness property and bioavailability character. Further, having high gastro intestinal absorption and high skin permeability which suggests that our novel compound acts as an antibacterial agent. The molecular dynamics simulation results of the protein-ligand complex show that the RMSD of the protein and ligand are nearly identical indicating that the ligand has excellent binding affinity with the protein.

Hence, based on the theoretical ideas the chemical and biological endeavours of the synthesized compound were investigated and further, biological studies helps us to design, explore and enhance the biological activity of the similar compounds.

CRediT authorship contribution statement

M. Hamsaveni: Writing – original draft, Visualization, Software, Investigation, Data curation. Ruthu Ramachandra Hegde: Visualization, Software, Investigation, Data curation. B. Sahana: Visualization, Software, Investigation, Data curation. B.S. Chethan: Methodology, Formal analysis, Conceptualization. K. Pruthviraj: Formal analysis. N. Maithra: Formal analysis, Conceptualization. D.C. Vinay Kumar: Methodology, Formal analysis, Conceptualization. S.V. Niranjana: Formal analysis. K. Sunil: Resources, Project administration. N.K. Lokanath: Writing – review & editing, Supervision, Resources.

Declaration of competing interest

The authors declare that they have no known competing financial

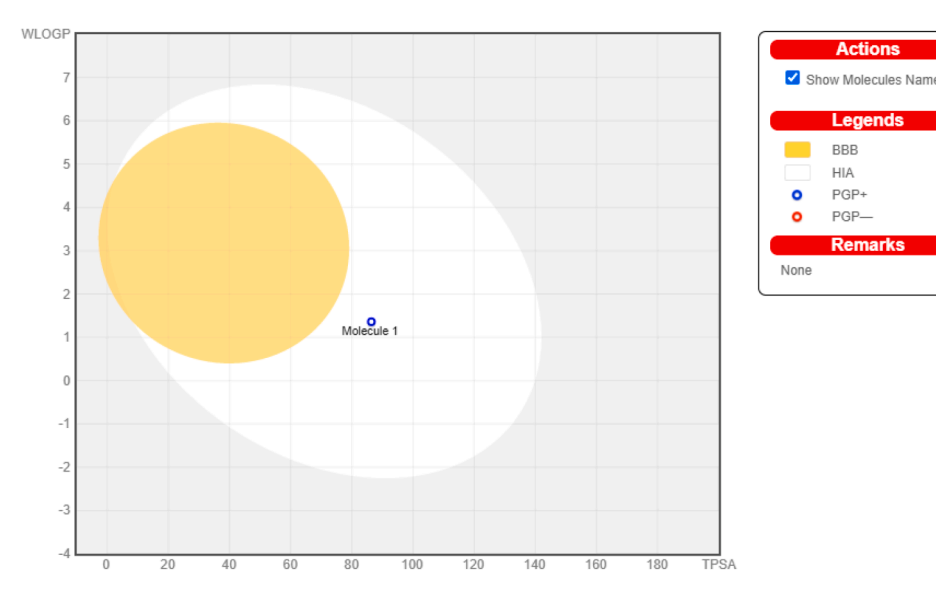


Fig. 18. Boiled Egg diagram of the synthesized compound showing high gastrointestinal permeation.

interests or personal relationships that could have appeared to influence the work reported in this paper.

Data availability

Data will be made available on request.

Acknowledgments

The authors are thankful to the DST-FIST (SR/FST/PSI-119/2019), National Single Crystal Diffractometer Facility, DoS in Physics, CPEPA, IOE and DST-PURSE, Vijnana Bhavan, University of Mysore, Mysuru for providing the instrumentation facility. The author Sunil. K is thankful to Sri Siddhartha Academy of Higher Education (SSAHE) and Karnataka Council for Technological Upgradation (KCTU).

Supplementary materials

Supplementary material associated with this article can be found, in the online version, at doi:10.1016/j.molstruc.2024.139367.

References

- N. Kerru, L. Gummidi, S. Maddila, K.K. Gangu, S.B. Jonnalagadda, A review on recent advances in nitrogen-containing molecules and their biological applications, Molecules 25 (2020), https://doi.org/10.3390/molecules25081909.
- [2] D.J. Newman, G.M. Cragg, Natural products as sources of new drugs from 1981 to 2014, J. Nat. Prod. 79 (2016) 629–661, https://doi.org/10.1021/acs. jnatprod.5b01055.
- [3] M.J. Robb, J.S. Moore, A retro-staudinger cycloaddition: mechanochemical cycloelimination of β-Lactam Mechanophore, Am. Chem. Soc. 137 (2015), https://doi.org/10.1021/jacs.5b07345.
- [4] M. Baiula, P. Galletti, G. Martelli, R. Soldati, L. Belvisi, M. Civera, S. Deianira Dattoli, S. Mario Spampinato, D. Giacomini, New β-lactam derivatives modulate cell adhesion and signaling mediated by RGD-binding and leukocyte integrins, J. Med. Chem. 59 (2016) 9721–9742, https://doi.org/10.1021/acs. imedchem.6b00576.
- [5] M.W. Majewski, P.A. Miller, A.G. Oliver, M.J. Miller, Alternate "drug" delivery utilizing β-lactam cores: syntheses and biological evaluation of β-lactams bearing isocyanate precursors, J. Org. Chem. 82 (2017) 737–744, https://doi.org/10.1021/ acs.joc.6b02272.
- [6] P. Karegoudar, M.S. Karthikeyan, D.J. Prasad, M. Mahalinga, B.S. Holla, N. S. Kumari, Synthesis of some novel 2,4-disubstituted thiazoles as possible antimicrobial agents, Eur. J. Med. Chem. 43 (2008) 261–267, https://doi.org/10.1016/j.eimech.2007.03.014.
- [7] A. Andreani, M. Rambaldi, A. Locatelli, R. Bossa, A. Fraccari, I. Galatulas, Potential antitumor agents. XX (1) 6-anilinoimidazo[2,1-b]thiazoles, Pharm. Acta Helv. 68 (1993) 21–24, https://doi.org/10.1016/0031-6865(93)90004-P.
- [8] C. Zhang, D.L. Zink, M. Ushio, B. Burgess, R. Onishi, P. Masurekar, J.F. Barrett, S. B. Singh, Isolation, structure, and antibacterial activity of thiazomycin A, a potent thiazolyl peptide antibiotic from Amycolatopsis fastidiosa, Bioorg. Med. Chem. 16 (2008) 8818–8823, https://doi.org/10.1016/J.BMC.2008.08.079.
- [9] A. Andreani, M. Granaiola, A. Leoni, A. Locatelli, R. Morigi, M. Rambaldi, Synthesis and antitubercular activity of imidazo[2,1-b]thiazoles, Eur. J. Med. Chem. 36 (2001) 743–746, https://doi.org/10.1016/S0223-5234(01)01266-1.
- [10] R.G. Kalkhambkar, G.M. Kulkarni, H. Shivkumar, R.N. Rao, Synthesis of novel triheterocyclic thiazoles as anti-inflammatory and analgesic agents, Eur. J. Med. Chem. 42 (2007) 1272–1276, https://doi.org/10.1016/J.EJMECH.2007.01.023.
- [11] A. Andreani, M. Rambaldi, A. Leoni, A. Locatelli, F. Andreani, J.C. Gehret, Synthesis of imidazo[2,1-b]thiazoles as herbicides, Pharm. Acta Helv. 71 (1996) 247–252, https://doi.org/10.1016/S0031-6865(96)00021-0.
- [12] Q. Wang, H. Li, Y. Li, R. Huang, Synthesis and Herbicidal Activity of 2-Cyano-3-(2-chlorothiazol-5-yl)methylaminoacrylates, J. Agric. Food Chem. 52 (2004) 1918–1922, https://doi.org/10.1021/jf035312a.
- [13] M. Robb. New chemistry with Gaussian 16 & GaussView 6, 2022. https://spiral.imperial.ac.uk/handle/10044/1/57650.

- [14] P.S.V. Kumar, V. Raghavendra, V. Subramanian, Bader's theory of atoms in molecules (AIM) and its applications to chemical bonding, J. Chem. Sci. 128 (2016) 1527–1536, https://doi.org/10.1007/s12039-016-1172-3.
- [15] U. Koch, P.L.A. Popelier, Characterization of C-H-0 hydrogen bonds on the basis of the charge density, J. Phys. Chem. 99 (1995) 9747–9754, https://doi.org/ 10.1021/j100024a016.
- [16] I. Rozas, I. Alkorta, J. Elguero, Behavior of ylides containing N, O, and C atoms as hydrogen bond acceptors, J. Am. Chem. Soc. 122 (2000) 11154–11161, https:// doi.org/10.1021/ja0017864.
- [17] T. Lu, F. Chen, Multiwfn: a multifunctional wavefunction analyzer, J. Comput. Chem. 33 (2012) 580–592, https://doi.org/10.1002/jcc.22885.
- [18] W. Humphrey, D. Andrew, S. Klaus, VMD: visual molecular dynamics, J. Mol. Graph. 14 (1996) 33–38, https://doi.org/10.1016/0263-7855(96)00018-5.
- [19] G.M. Morris, D.S. Goodsell, R.S. Halliday, R. Huey, W.E. Hart, R.K. Belew, A. J. Olson, Automated docking using a Lamarckian genetic algorithm and an empirical binding free energy function, J. Comput. Chem. 19 (1998) 1639–1662, https://doi.org/10.1002/(SICI)1096-987X(19981115)19:14<1639::AID-JCC10>3.0.CO;2-B.
- [20] D Studio, Discovery studio, Accelrys 2.1 (2008) 420.
- [21] M. Nagaraju, C.S. Karthik, M.K. Hema, B.S. Chethan, R.J. Ramalingam, M. Karnan, N.K. Lokanath, Perusal on the role of DMF solvent and hydrogen bonding in the formation of 1D polymeric chains in mixed ligand Ni(II) complex as an anticancer agent: a computational approach, J. Biomol. Struct. Dyn. (2023), https://doi.org/10.1080/07391102.2023.2291543.
- [22] D.C. Vinay Kumar, B.S. Chethan, S. V, K.S. Rangappa, N.K. Lokanath, Structural elucidation and in-silico evaluation of 1,2,4-triazole derivative as potent Omicron variant of SARS-CoV-2 spike protein inhibitor with pharmacokinetics ADMET and drug-likeness predictions, J. Mol. Struct. 1297 (2024) 136976, https://doi.org/ 10.1016/J.MOLSTRUC.2023.136976.
- [23] R. Parthasarathi, V. Subramanian, D.R. Roy, P.K. Chattaraj, Electrophilicity index as a possible descriptor of biological activity, Bioorg. Med. Chem. 12 (2004) 5533–5543, https://doi.org/10.1016/J.BMC.2004.08.013.
- [24] A. Savin, R. Nesper, S. Wengert, T.F. Fässler, ELF: the electron localization function, Angew. Chem. 36 (1997) 1808–1832, https://doi.org/10.1002/ anie.199718081 (International Edition in English).
- [25] H.L. Schmider, A.D. Becke, Chemical content of the kinetic energy density, J. Mol. Struct. THEOCHEM 527 (2000) 51–61, https://doi.org/10.1016/S0166-1280(00) 00477-2.
- [26] S. De Falco, The discovery of placenta growth factor and its biological activity, Exp. Mol. Med. 44 (2012) 1–9, https://doi.org/10.3858/emm.2012.44.1.025.
- [27] A. Daina, O. Michielin, V. Zoete, SwissADME: a free web tool to evaluate pharmacokinetics, drug-likeness and medicinal chemistry friendliness of small molecules, Sci. Rep. 7 (2017), https://doi.org/10.1038/srep42717.
- [28] F. Batool, E.U. Mughal, K. Zia, A. Sadiq, N. Naeem, A. Javid, Z. Ul-Haq, M. Saeed, Synthetic flavonoids as potential antiviral agents against SARS-CoV-2 main protease, J Biomol. Struct. Dyn. 40 (2022) 3777–3788, https://doi.org/10.1080/ 07391102.2020.1850359.
- [29] A. Abdou, Synthesis, structural, molecular docking, DFT, vibrational spectroscopy, HOMO-LUMO, MEP exploration, antibacterial and antifungal activity of new Fe (III), Co(II) and Ni(II) hetero-ligand complexes,, J. Mol. Struct. 1262 (2022) 132911, https://doi.org/10.1016/J.MOLSTRUC.2022.132911.
- [30] S. Celik, S. Akyuz, A.E. Ozel, Structural and vibrational investigations and molecular docking studies of a vinca alkoloid, vinorelbine, J. Biomol. Struct. Dyn. (2023) 9666–9685, https://doi.org/10.1080/07391102.2022.2145369.
- [31] M. Rizwan, S. Ali, S. Shahzadi, S.K. Sharma, K. Qanungo, M. Shahid, S. Mahmood, Synthesis, characterization, HOMO-LUMO study, and antimicrobial activity of organotin (IV) complexes of 4-piperidine carboxamide and its Schiff base, J. Mol. Struct. 1258 (2022) 132693, https://doi.org/10.1016/J. MOLSTRUC.2022.132693.
- [32] S. Celik, S. Akyuz, A.E. Ozel, Vibrational spectroscopic characterization and structural investigations of Cepharanthine, a natural alkaloid, J. Mol. Struct. 1258 (2022) 132693, https://doi.org/10.1016/J.MOLSTRUC.2022.132693.
- [33] S. Murugavel, N. Manikandan, D. Lakshmanan, K. Naveen, P. Thirumalai Perumal, Synthesis, crystal structure, dft and antibacterial activity studies of (E)-2-benzyl-3-(Furan-3-yl)-6,7-dimethoxy-4-(2-Phenyl-1h-inden-1-ylidene)-1,2,3,4tetrahydroisoquinoline, J. Chil. Chem. Society. 60 (2015) 3015–3020, https://doi. org/10.4067/S0717-97072015000300008.
- [34] M. Ismail, R. Ahmad, A. Latif, A. Khan, A. Alam, F.A. Ozdemir, Ammara, M. Ali, Synthesis, antibacterial activities and theoretical study of Polyhydroquinoline derivatives, ChemistrySelect (2023), https://doi.org/10.1002/slct.202300954.
- [35] S. Celik, S. Akyuz, A.E. Ozel, Molecular modelling, DFT quantum chemical analysis, and molecular docking on edotecarin, an indolocarbazole anticancer agent, J. Mol. Liq. (2022) 27–49, https://doi.org/10.1080/ 15421406.2022.2084240.